DOI: ADD DOINUMBER HERE

Reduction of Solid Propellants Environmental Impact: Al-Mg Mechanically Activated Fuels and AP-PSAN Blends

Christian Paravan[⋆†], *Stefano Dossi*[⋆⋆], *Filippo Maggi*[⋆], *Luciano Galfetti*[⋆]
Alexander B. Vorozhtsov[⋆⋆⋆], *Ilya Zhukov*[⋆⋆⋆], *Sergej Sokolov*[⋆⋆⋆]
[⋆]*Politecnico di Milano*
20156 Milan, Italy
[⋆⋆]*ReActive - Powder Technology srl*
20158 Milan, Italy
[⋆⋆⋆]*National Research Tomsk State University*
634050 Tomsk, Russian Federation
[†]Corresponding Author: christian.paravan@polimi.it

Abstract

The work focuses on the use of composite *Al-Mg* powders in solid propellants based on ammonium perchlorate (*AP*)-phase stabilized ammonium nitrate (*PSAN*) blends. The combination of blended oxidizer and bi-metal powders tackles the issue the *HCl* emissions from solid propellants. Composite powders are produced by different mechanical activation processes. Exploiting the flexibility of these methods, metal fuels with *Mg* mass fractions of 30% and 50% are realized and tested. Experimental investigation includes powders pre-burning characterization, propellant combustion tests and combustion surface visualizations for the analysis of incipient aggregation/agglomeration.

1. Introduction

Solid propellants are mature systems playing a key role for launch applications. This central position has been gained through years of continuous development and three main pillars: (*i*) the availability of suitable binders providing high enough mechanical properties also in the case of high filler loads [1, 2], (*ii*) the use of ammonium perchlorate (*AP*) as oxidizer [3], and (*iii*) the performance tailoring offered by metal fuels and, in particular, by *Al* powders [4]. In spite of its suitable characteristics (in particular, the favorably high oxygen balance), *AP* implies the presence of *Cl* in the solid propellant exhaust. In particular, the main drawback of *AP*-based commercial solid propellants is the presence of a significant mass fraction of *HCl* in the exhaust products. Thermochemical equilibrium calculations identify nearly 20 *wt%* of *HCl* in the plume of solid rocket motors with *AP* loads in the (typical) range 65-70 *wt%*. Propulsion grade *Al* powder is typically micron-sized (μAl), with relatively high metal content favoring increased gravimetric (and volumetric) specific impulse (I_{sp}). The actual specific impulse of *Al*-loaded propellants is influenced by the presence of two-phase flow losses originated by the presence of condensed combustion products (*CCP*) and by metal combustion process. Micron-sized *Al* combustion implies aggregation/agglomeration phenomena [5, 6, 7, 8, 9, 10]. Agglomerates are responsible for performance losses (incomplete metal combustion, kinetic and thermal lags in the expanding gaseous propellant). The aggregation/agglomeration process is affected by factors as the propellant composition, microstructure and burning rate (r_b) [7, 11].
Ammonium nitrate (*AN*) is a *Cl*-free candidate for *AP* (total/partial) substitution in solid propellants [12]. This process is hindered by inherent difficulties [12, 13]: (*i*) *AN* is highly hygroscopic (thus, strict storage and handling conditions are required), (*ii*) *AN* features a reduced oxygen balance with respect to *AP*, (*iii*) pure *AN* is subject to crystalline-phase transitions at relatively low temperature (and this transformation is affected by humidity), (*iv*) combustion mechanism affected by liquid layer formation. A suitable method for the augmentation of *AN* thermal stability is the use of phase-stabilized *AN* (*PSAN*). Mitigation of the issues related to the combustion process of *AN*/*PSAN* can be obtained by metal fuels featuring enhanced reactivity and more prompt ignition/combustion. Such a strategy offers attractive possibilities also for the reduction of the size of *CCP* leaving the burning surface as a consequence of aggregation/agglomeration phenomena. Focusing on *Al* as the main fuel ingredient, the pursuit of enhanced reactivity yields the interest for non-convetional fuels as nano-sized or activated powders.
Nano-sized *Al* (*nAl*) offers high reactivity (i.e, lower ignition temperature and higher $Al \rightarrow Al_2O_3$ conversion) thanks

to its large specific surface area (SSA) [14, 15, 16, 17]. This increased reactivity turns to (*i*) significant r_b enhancement, and (*ii*) CCP size reduction. Yet, ultradisperse fuel particle sizes imply an increase in the viscosity of propellant slurries with high nAl mass fractions and (for air-passivated powders) a reduction of the active aluminum content (C_{Al}) of the propellant (a factor suggesting, for application to commercial launch systems, a proper trade-off between nAl mass fraction in the propellant, and I_{sp}) [4]. In addition to this, nano-sized powders require well controlled storage conditions and complex handling/manufacturing, or surface treatments [14, 18, 19, 20, 21].
Mechanical activation (MA) is a promising technique for the production of innovative metal fuel powders: composition, size, shape, and reactivity of the particles can be tailored by the process. The most significant advantage of powders from MA is that they retain size in the micrometric range but with enhanced reactivity over conventional powders thanks to the composition/morphology changes. Mechanical activation enables the creation of powders with dual composition: this is an attractive feature for the creation of metal fuels combining the characteristics of different materials as, for example, the high energy release of Al with the easy ignition and combustion of Mg. Discussions of composite aluminum-magnesium powders are reported in Refs. [22, 23, 24, 25, 26]

This work discusses recent results obtained in a collaboration program involving the $SpacePropulsionLaboratory$ ($SPLab$) of $PolitecnicodiMilano$, the $TomskStateUniversity$ (TSU) and *ReActive - Powder Technology s.r.l.*, a spin-off company of $PolitecnicodiMilano$. The work focuses on the use of composite Al-Mg powders in AP-$PSAN$ solid propellants. Composite Al-Mg powders are produced by MA, but differ for their composition, for the specific activation procedure and for the post-activation treatments and feature different compositions. Powders are tested in a pre-combustion phase, and are then used in propellants with different compositions. For the investigated propellants, burning behavior is assessed considering quasi-steady burning rate (r_b) under different combustion chamber pressures (p), and burning surface visualizations highlighting incipient aggregation/agglomeration phenomena.

Metal powders are supplied by TSU, and *ReActive - Powder Technology s.r.l.*. Powder characterization and burning tests are performed at $SPLab$.

2. Experimental Strategy and Methods

The logical path for the development of the work is the following: (*i*) theoretical analyses based on $NASA-CEA$ code, (*ii*) pre-burning characterization of the powders, (*iii*) burning behavior investigation of selected propellant formulations.

The $NASA-CEA$ is used to evaluate the impact on propellant performance (i.e., I_{sp}, HCl emissions), of two main factors: (*i*) $Al-Mg$ composite composition, and (*ii*) partial substitution of AP with $PSAN$.
Pre-burning characterization of the powders aims to identify powder characteristics to support the analysis of evidences from the burning tests.
The combustion analysis is divided into two parts. In a first analysis, propellants with low metal mass fraction are analyzed. A second test campaign involves propellant formulations with 18 *wt%* metal. The choice for a burning behavior investigation divided into two parts is related to the relatively small amount of material available for testing, and the possibility of a wider relative grading of different additives spanning from nAl and including the $Al-Mg$ powders, given the availability of previous data.

Pre-burning characterization of the powders is performed by scanning electron microscopy (SEM), particle size distribution (PSD), and simultaneous thermal analysis (differential scanning calorimetry-thermogravimetry, $DSC-TG$). Burning tests provide burning rate as a function of chamber pressure, together with combustion surface visualization. Electron microscopy analyses are performed by a Hitachi $TM3000$ SEM. Average particle size and size-distribution analyses are performed by Malvern $Mastersizer$ 2000 with dry dispersion unit. Slow heating rate oxidation behavior of the powders is investigated by Netzsch $STA449$ $Jupiter$ $F5$ (air, 0.1 MPa, 20 ml/min, 10 K/min, from 300-1300 K). Active metal content of the powders is determined by a volumetric method measuring the H_2 gas evolution from metal-H_2O reaction. Basic (5 *wt% NaOH*) or acid (5 *wt% HCl*) water solutions are used based on the metal reaction of relevance.
Quasi-steady burning rate (r_b) and surface visualization analyses are performed in a windowed combustion chamber operating under quasi-steady combustion chamber pressure (p). Details on the test rig are given elsewhere [4, 8, 27]. Burning rates are measured by a non intrusive optical technique developed by $SPLab$ and based on video recording of the combsution process (125-250 fps, FastCam) [4, 8]. Burning surface visualization, with identification of incipient detachment of agglomerates and condensed combustion products visualization are performed by Phantom $V710$ high-speed camera (> 1000 fps) [4]. Details of the video recording process depends on the propellant burning charac-

teristics.

3. Thermochemical Analysis

Propellant theoretical performances are investigated by $NASA-CEA$ code. Calculations are performed with $p = 70$ bar, exhaust supersonic area ratio of 40, and shifting equilibrium through the nozzle. The main observable of interest are the specific impulse in vacuum ($I_{sp,vac}$, that is selected as a relevant parameter for relative grading purposes) and the HCl mass fraction at the throat section (MF_{HCl}). The latter is taken as an indicator of the environmental impact of the propellant formulation. A conventional commercial propellant formulation is taken as reference for the calculations. This baseline is composed by AP (68 $wt\%$), Al (18$wt\%$), and hydroxyl-terminated polybutadiene ($HTPB$, 14 $wt\%$). Data for the $HTPB$ heat of formation are taken from Ref. [3], the other ingredients (including the AN) are taken from $NASA-CEA$ database. The performed analysis does not consider the phase stabilization of the AN, since stabilizers have no marked effects on the thermochemical perfomance (in particular, when dealing with reltive gradings). In the analyses, the oxidizer-to-binder ratio is kept constant, as well as the metal fuel mass fraction. Metal fuel composition is changed between the different cases, moving from the extreme cases of Al and Mg. Results are presented in Figure 1, and Figure 2. Data from Figure 1a show $I_{sp,vac}$ reduction for increasing AN and Mg mass fraction. This is a

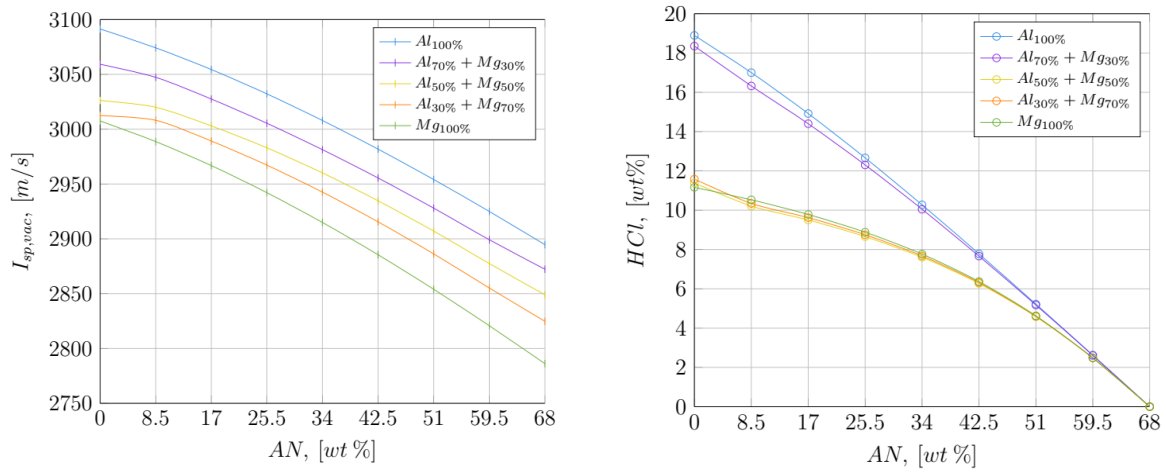

(a) (b)

Figure 1: NASA CEA results, dependence on AN mass fraction of parameters of interest: (a) specific impulse, and (b) HCl concentration at throat for propellant formulations with different AP + AN content.

consequence of the Cl-free oxidizer oxygen balance, and of Mg oxidation enthalpy (that is lower than that of Al, 24.7 MJ/kg for the former vs. 31.1 MJ/kg for the latter). Under the investigated conditions, the $I_{sp,vac}$ difference widens as the AN mass fraction increases. Considering the limiting cases of full substitution of Al with Mg, the difference is of 2.7% with AP as the oxidizer, and of 3.7% for 68 $wt\%$ AN. In an Al-loaded propellant, $I_{sp,vac}$ variation is from 3091 m/s to 2895 m/s in the case of a full AP substitution with AN, while a change from 3007 m/s to 2786 m/s is achieved when Mg is the only fuel.

Considering AP-based propellants loaded with Al + Mg powders, with a composite metal mass fraction of 18%, the $I_{s,vac}$ decreases by 1.0% when the powder contains 30 $wt\%$ Mg and of 1.9% when 50 $wt\%$ Mg is present (see Figure 1a). Under the investigated operating conditions, for the baseline propellant the HCl mass fraction at throat resulting from the thermochemical analyses is 18.9%. As shown in Figure 1a, this reduces to 17.8% and 11% for 70 $wt\%$ Al + 30 $wt\%$ Mg and 50 $wt\%$ Al + 50 $wt\%$ Mg, respectively. Such a reduction of the HCl, due to the Mg + Cl oxidation, is enhanced by the partial substitution of AP with AN. Data from Figure 1b show how a 51 $wt\%$ AP + 17$wt\%$ AN (thus, a 25% reduction of NH_4ClO_4 in the starting propellant formulation) reduces the HCl mass fraction at throat from the initial 18.9% to 14.4% for a metal fuel composed by 70 $wt\%$ Al + 30 $wt\%$ Mg, and to 9.5% when considering 50 $wt\%$ Al + 50 $wt\%$ Mg. The results come with a $I_{s,vac}$ of 3028 m/s (-2.0% with respect to the baseline) for a propellant loaded with 18 $wt\%$ 70 $wt\%$ Al + 30 $wt\%$ Mg. A propellant loaded with a composite 50 $wt\%$ Al + 50 $wt\%$ Mg yields 3003 m/s with a percent difference over the baseline of -2.8%.

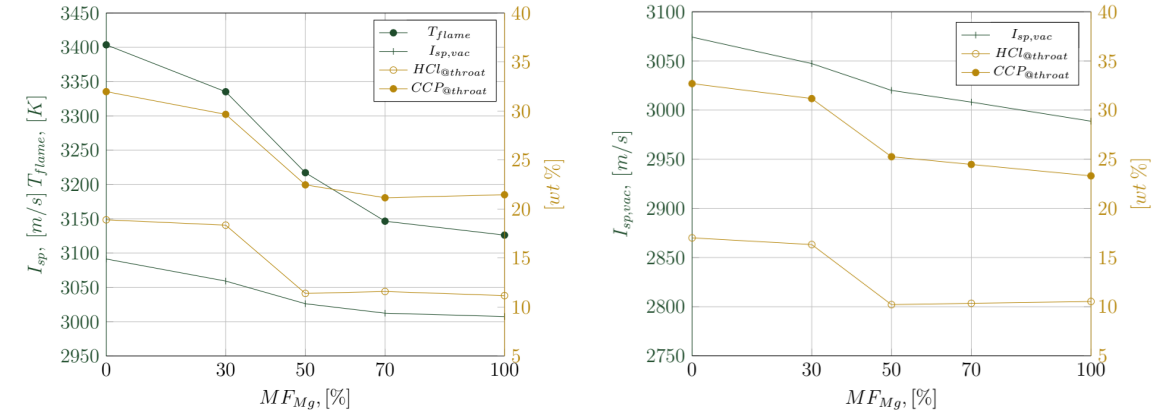

(a) (b)

Figure 2: NASA CEA results, dependence on Mg mass fraction of parameters of interest: adiabatic flame temperature, specific impulse, and HCl concentration at throat for propellant formulations with (a) 68 $wt\%$ AP, and (b) 51 $wt\%$ AP + 17 $wt\%$ AN.

Figure 2a,b show the vacuum specific impulse, the flame temperature (T_{flame}), the CCP emission, and the HCl produced by from relevant propellant formulations.

Actual Al-loaded commercial solid propellant performance feature a (nearly) 3% losses in terms of specific impulse due to two-phase flow. Use of Mg as an additive in composite powders promise easier ignition and more prompt combustion of the metal fuel, possibly lowering the size of condensed products originated by aggregation/agglomeration. For the aforementioned analyses, a propellant combining (i) partial AP substitution with AN, (ii) use of composite fuel powders with Mg content $\leq$ 50 $wt\%$, should exhibit a general set of suitable properties for applications granting burning performance and environmental impact reduction.

4. Investigated Materials

4.1 Oxidizers

Ammonium perchlorate (NH_4ClO_4) is supplied through $AvioS.p.A.$. The material is provided with a nominal particle size of 200 μm and it is used as it is, or after grinding and sieving. The latter procedures reduce the particle size of the initial AP crystals down to the nominal value of 20 μm. Thus, AP in the propellant is indicated as $coarse$ or $fine$, based on the particle size (see Table 1).

Powder Id.	$d_{0.5}$ μm	**Span**	D_{43}, μm
AP_{Coarse}	201	1.18	215
AP_{Fine}	10.1	4.74	18.9
$PSAN_{Coarse}$	86.3	2.49	114
$PSAN_{Fine}$	51.2	2.53	51.2

Table 1: Ammomium perchlorate and phase-stabilized ammonium nitrate PSD [D_{43} = average mass-based diameter, [4]; $d_{0.5}$ = median of the PSD; $Span = (d_{0.9} - d_{0.1})/d_{0.5}$, with $d_{0.9}$ and $d_{0.1}$ diameters below which 90% and 10% of the particle population lays, respectively].

Ammonium nitrate (NH_4NO_3) is obtained through $Fraunhofer\ ICT$ (Pfintzal, Germany). This oxidizer is phase stabilized by KNO_3 (7 $wt\%$). As for the AP, two different PSD of $PSAN$ are considered in the study, though crystal size is not strictly related to the burning behavior, in this case.

4.2 Binder

Hydroxyl-terminated polybutadiene ($HTPB$) is considered as binder in the formulations. The starting pre-polymer is supplied by $Avio\ S.p.A.$. The binder is plasticized by dyoctil-adipate (DOA), and cured with isophorone di-isocyanate ($IPDI$). The hydroxyl functionality of the $HTPB\ R45$ is 2.352, while the binder curing ratio ($[-NCO]/[-OH]$) is 1.04.

4.3 Metal Powders

The investigated metal powders are presented in Table 2. $Act-AlMg$-powders are produced by *ReActive - Powder technology s.r.l.*. For these products, the starting material details are available, while for the $AlMg-50$ by TSU, only the final product was available.
Relevant data for the starting materials are reported in Table 2. The micron-sized Al (nominal particle size of 30 μm) is produced by $AMG-Alpoco$ (Rotherham, UK), while the Mg powder (nominal particle size 44 μm is supplied by $Merck\ KGaA$ (Darmstadt, Germany). The reference Al powder has an actual particle size well meeting the nominal

Powder Id.	$\mathbf{d}_{0.5}$,μm	**Span**	$\mathbf{D}_{43}$,μm	C_{Me}, $wt\%$
Al	39.0	1.67	44.2	99.5 ±0.7
Mg	35.6	1.35	38.8	93.4 ±1.5
$AlMg-50$	16.3	2.63	21.6	90.7 ±2.4
$Act-AlMg-50$	37.9	2.38	40.5	91.9 ±1.8
$Act-AlMg-70$	46.5	2.44	60.6	90.5 ±1.5

Table 2: Relevant size and composition data for the metal powders. Note that PSD for the $Act-AlMg-50$ and $Act-AlMg-50$ feature flake particles while $Mastersizer$ 2000 evaluates size distribution for spherical and smoot spheres.

Powder Id.	$T_{Onset,1}$, K	$T_{Onset,2}$, K	α_{933K}, %	α_{1273K}, %
Al	865.0	1225	3.0	3.5
Mg	814.6	–	65.2	99.5
nAl	848.3	1022.0	29.0	69.3
$AlMg-50$	781.2	954.8	–	–
$Act-AlMg-50$	718.0	886.2	39.4	68.0
$Act-AlMg-70$	874.7	958.3	24.8	62.2

Table 3: Reactivity parameters from $DSC-TG$ (air, 20 ml/min, 0.1 MPa, 10 K/min). Conversion factor (α_T), is defined based on metal conversion into oxide, considering the powder composition and active metal content [28]. Note that nAl data are limited to 1173 K.

value. The median of the PSD (39 μm) is in agreement with the declared 30 μm. The active metal content is very high, thanks to the small influence of the (relatively thin) alumina layer surrounding the metal core. Particles feature a spherical/spheroid shape, as shown by the SEM images of the Figure 3. The Mg powder show similar nominal and actual average particle sizes. Size distribution is relatively uniform, as shown by the span and the D_{43} values. Scanning electron microscope images of the Mg are reported in Figure 4.
Thermal analysis data for the Al and Mg powders are reported in Table 3, where data for a nAl powder with nominal size of 100 nm (SSA = 12.6 m^2/g, C_{Al} = (82.8 ± 0.2)$wt\%$) are reported for comparison. Reactivity parameters are evaluated as in Ref. [19]. Under the investigated conditions, the more prompt oxidation of Mg is well captured by the reactivity parameters showing more marked mass gains and conversion factors for this metal than for Al.
Composite powders data are reported in Table 2 and in Table 3. The $AlMg-50$ is produced by a spheridization process of previously milled powders. The SEM images of Figure 5 show relatively small particles with rounded edges. The powder $DSC-TG$ shows an endothermic peak at 735 K, which suggests the presence of the intermetallic phase β Mg_2Al_3.

The $Act-AlMg$ powders are produced by high-energy mechanical activation and feature a flake-like shape (see Figure 6). Due to this, data from Table 2 should be considered mainly for a relative grading between the mechanically activated powders rather than as absolute values (PSD from $Mastersizer$ 2000 is evaluated considering smooth, spherical particles). As shown by the images in Figure 6d, the Feret's diameter of the particles of $Act-AlMg-70$

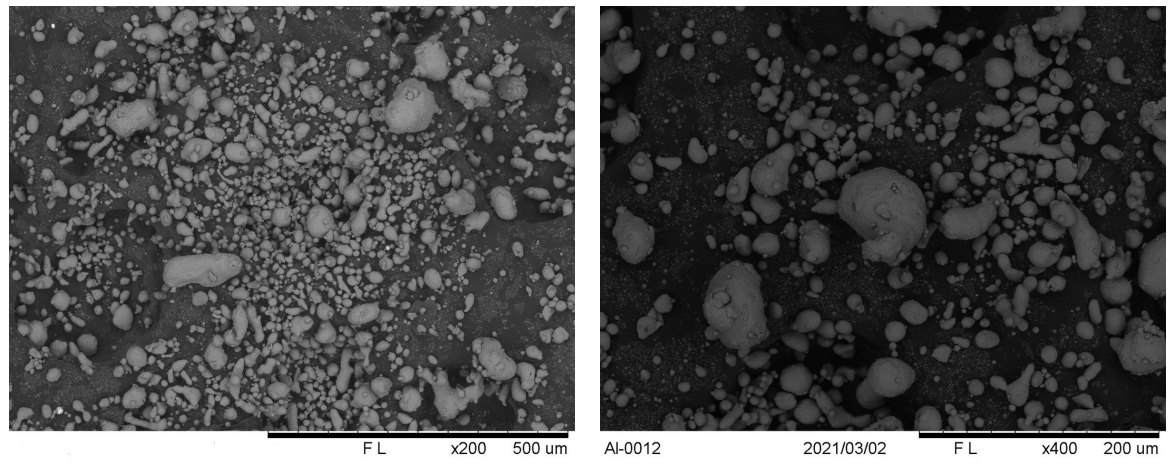

(a) (b)

Figure 3: SEM images of the starting reference Al powder (starting material for the activated composites).

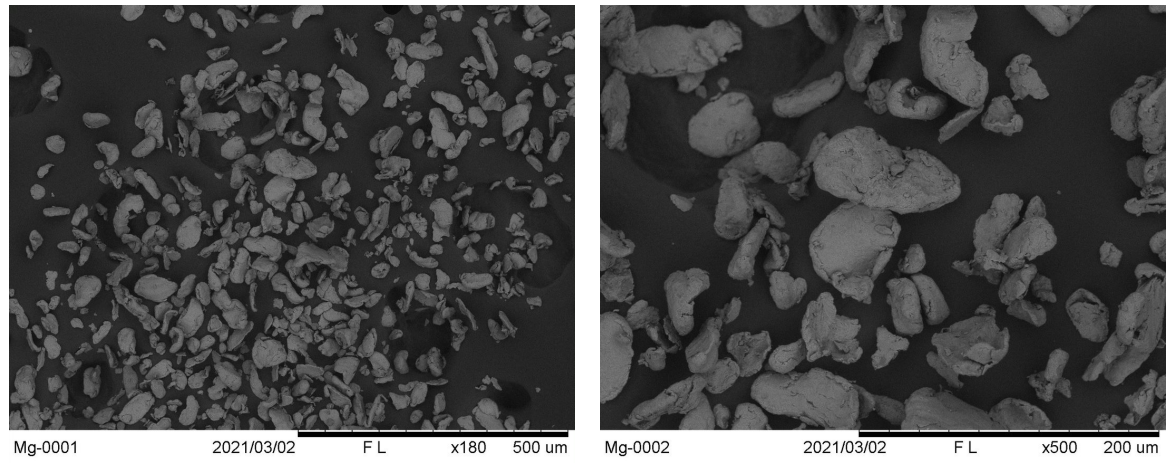

(a) (b)

Figure 4: SEM images of the starting Mg powder (starting material for the activated composites).

can be in the order of 150 μm. Slow oxidation in air of the composite powders show that, irrespective of the starting material/manufacturing process, the higher the Mg mass fraction, the earlier the intense onset of the first oxidation. For the $AlMg-50$ the metal-to-oxide conversion is 95.4%, while the flake powders show limiting values in the range 57.6% to 60.1%, with the higher result achieved by the $Act-AlMg-50$. All the composite powders feature a double oxidation peak. Thus, it is a likely effect of the presence of Mg, though, for the mechanically activated powders, an influence of the particle morphology is also likely.

5. Combustion Tests Results and Discussion

Table 4 summarizes the tested propellant formulations considered in the two steps of the analysis. Relevant data are discussed in the following subsections. All the tested propellants are produced by $SPLab$-developed procedures, exploiting resonant acoustic mixing. The propellants feature actual desnisties < 1.5% with respcet to the theoretical maximum desisty (TMD).

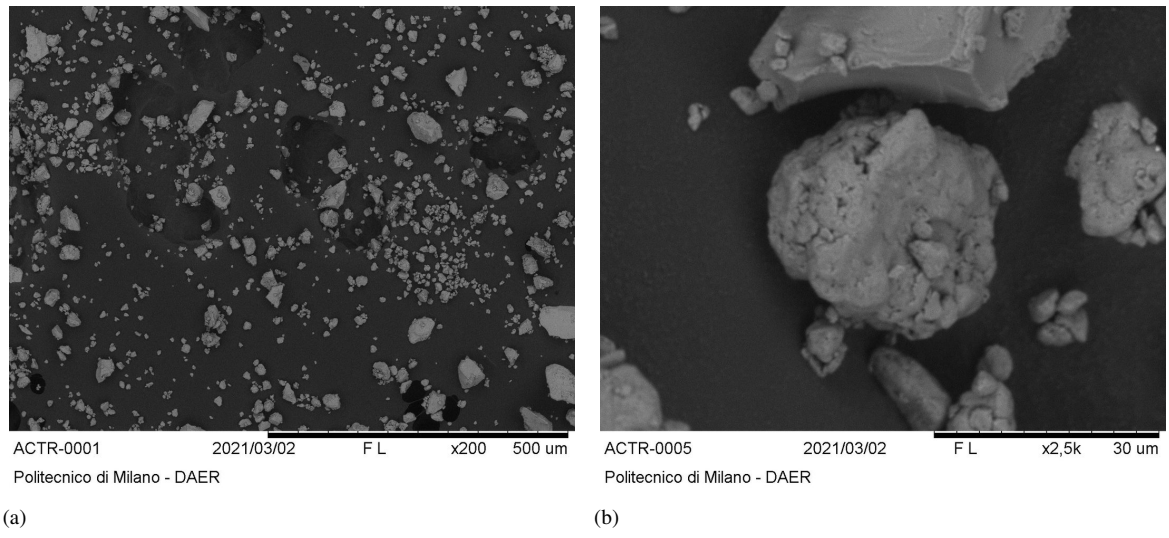

(a) (b)

Figure 5: SEM images of the $AlMg-50$.

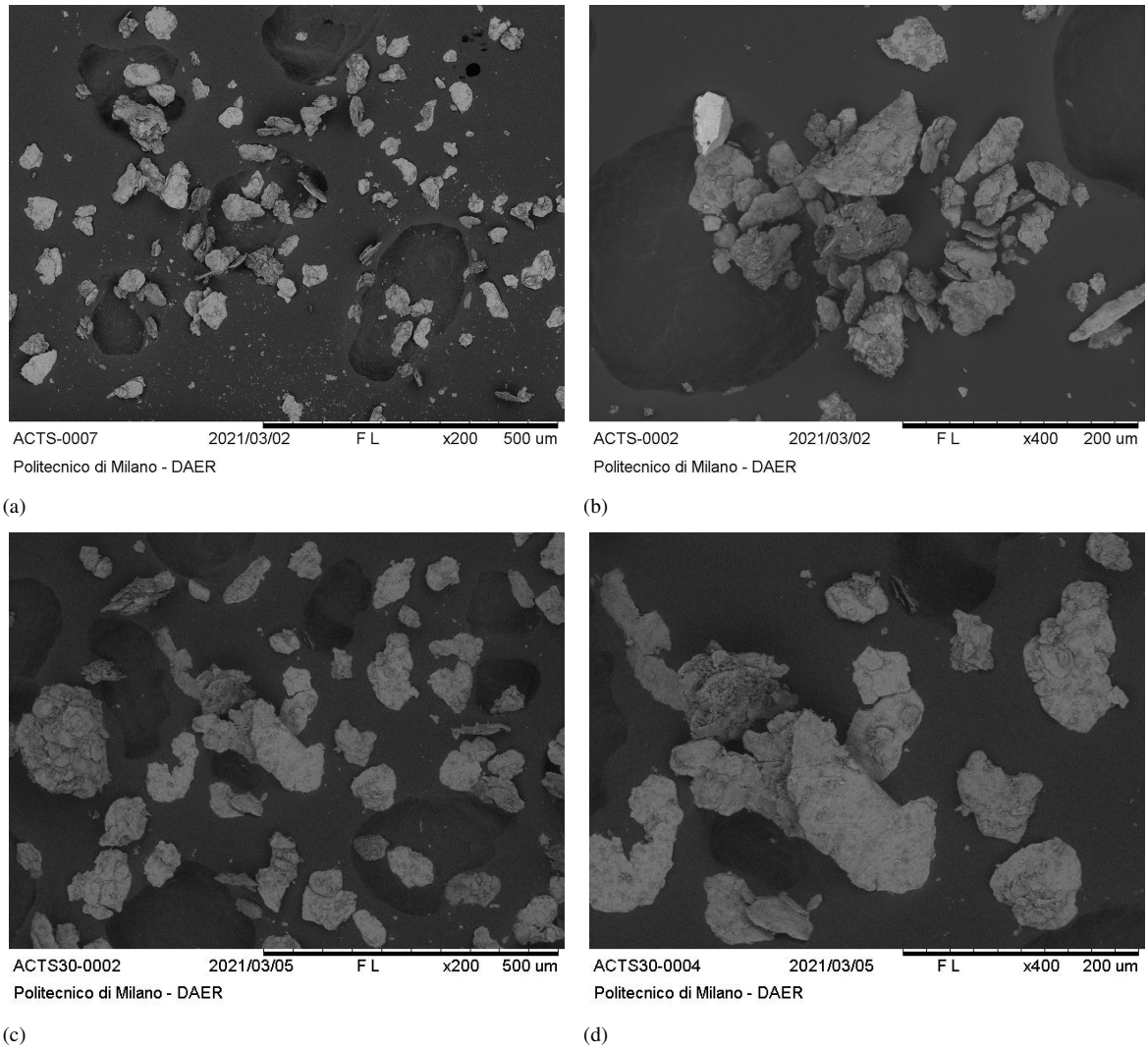

(a) (b)

(c) (d)

Figure 6: SEM images of (a,b) $Act-AlMg-50$, (c,d) $Act-AlMg-70$.

Propellant Id.	**Metal Fuel,** *wt%*	AP_{coarse}**,** *wt%*	AP_{fine}**,** *wt%*	$PSAN$**,** *wt%*	$HTPB$**,** *wt%*
$SP-1$	Al, 6.6	66.0	10.1	–	17.3
$SP-2$	Mg, 6.2	66.3	10.2	–	18.3
$SP-3$	$AlMg-50$, 6.3	66.2	10.2	–	17.3
$SP-4$	$Act-AlMg-50$, 6.4	66.1	10.2	–	17.3
$SP-0$	nAl, 8.0	65.0	10.0	–	17.0
$SP-1B$	Al, 18.0	41.0	10.0	17.0	14.0
$SP-4B$	$Act-AlMg-50$, 18.0	41.0	10.0	17.0	14.0
$SP-5B$	$Act-AlMg-70$, 18.0	41.0	10.0	17.0	14.0

Table 4: Tested propellant formulations.

5.1 Metallized Propellants: Relative Ballistic Grading

In this Section analysis is focused solid propellant formulations from $SP-1$ to $SP-5$ (see Table 4.Relative grading of the tested formulations is presented in Figure 7. For $SP-0$, that is included in the analysis for a more complete discussion, Vieille's law is $(1.479 \pm 0.110)^{(0.553\pm0.024)}$, with data fitting ($R^2$) of 0.982.
Relative ballistic grading of the tested formulations is presented in terms of percent burning rate increase in Table 5.

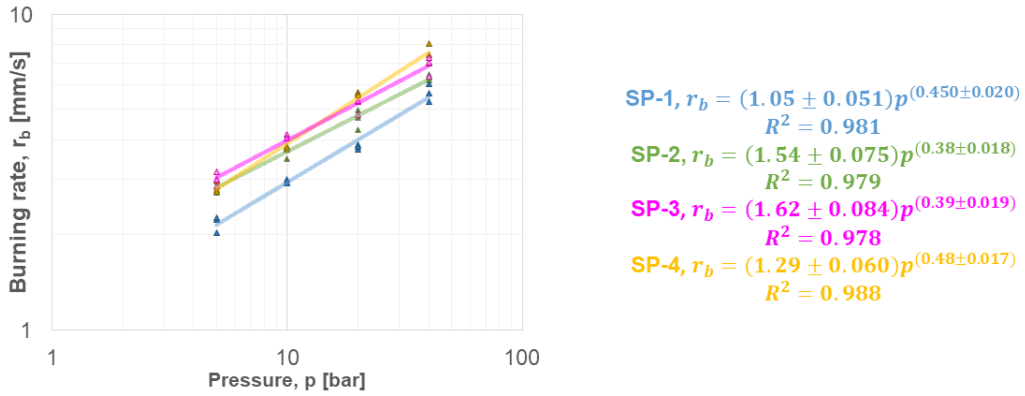

Figure 7: Relative ballistic grading of propellants with equimolar metal fuel content. Reference formulation for molar content definition is $SP-0$.

Data from Figure 7 and Table 5, show the benefits in terms of r_b due to the use of Mg at relatively low pressures.

Propellant Id.	p **= 10** *bar*	p **= 20** *bar*	p **= 40** *bar*
$SP-2$	+24	+23	+12
$SP-3$	+38	+35	+22
$SP-4$	+27	+47	+33
$SP-0$	+78	+92	+106

Table 5: Burning rate percent differences with respect to the baseline ($SP-1$).

Under the investigated conditions, this burning rate enhancement is gradually lost as pressure increases. The $SP-3$ show a r_b enhancement over the baseline of 38% at 10 *bar*, while the propellant loaded with $Act-AlMg-50$ is limited to +27%. As the pressure increases, the performance enhancement of $SP-4$ becomes stronger, with a +33% at 40 *bar* (see Table 5). This is well captured by the Vieille's laws showing ballistic exponents of 0.39 and 0.48 for $SP-3$ and $SP-4$, respectively.

5.2 Propellants based on $AP-PSAN$ Blend: Relative Ballistic Grading

In this Section analysis is focused solid propellant formulations from $SP-1B$ to $SP-5B$ (see Table 4.Relative grading of the tested formulations is presented in Figure 8. Data are limited to $Act-AlMg$-loaded propellants, due to criticalities encountered in the curing of the formulation loaded with $AlMg-50$. Percent differences in the r_b of the tested formulations is shown in Table 6.

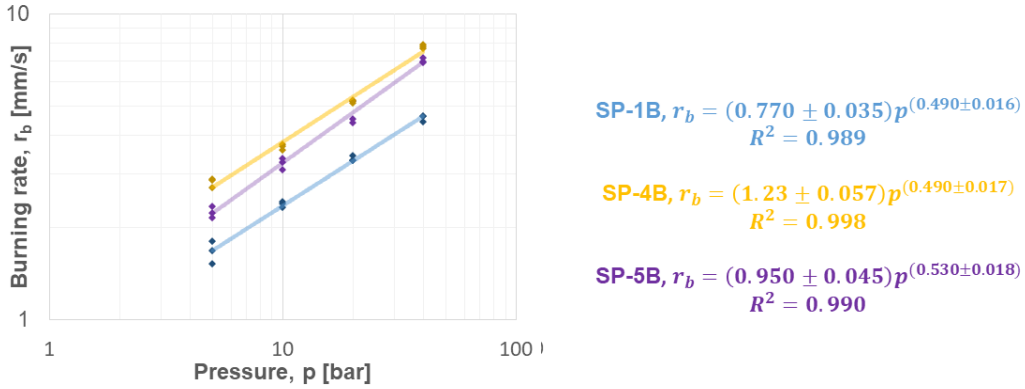

Figure 8: Relative ballistic grading of propellants with $AP-PSAN$ blend.

Propellant Id.	p **= 10** bar	p **= 20** bar	p **= 40** bar
$SP-4B$	+60	+60	+60
$SP-5B$	+35	+39	+43

Table 6: Burning rate percent differences with respect to the baseline ($SP-1B$).

The ballistic response of $SF-1B$ shows a 22.5% reduction in the burning rate, with respect to the case of a conventional commercial propellant (see Ref. [27]).This result is achieved in spite of the benefits of Mg addition to the r_b that are testified by the SF-4B and SF-5B data in Table 6. Percent r_b increases of $SP-4B$ are constant over the investigated p range, due to the ballistic exponent value of this formulation, that is the same as the baseline, under the investigated conditions (see Table 8). Moreover, the higher Mg mass fraction favors the Al combustion promoting faster burning rates with respect to $SP-5B$.

5.3 Propellant Burning Surface Visualizations

Propellant burning surface visualization provide condensed combustion products size (and, possibly, morphology), together with details of the combustion process. The analysis of the agglomerates in incipient detachment from the burning surface is performed collecting data for (at least) 200 particles [4]. Particle sizes are presented as D_{43} for spherical objects, while a representative size is given for (apparently) flake/non-spherical particles. An overview of the results is presented in Table 7. A series of images showing the detachment burning metal particles from the combustion surface is shown in Figures 9, 10, 11.

Propellant Id.	CCP **Size,** μm	**Notes**
SP-1	85.5 ±12.5	D_{43}
SP-4	306 ±16	Apparently flake particle
SP-1B	210 ±16	D_{43}, Note that for an AP-based propellant: D_{43} = 86.2 ±3.0, [27].
SP-4B	323 ±15	Apparently flake particle

Table 7: Measured CCP size ($p = 10$ bar).

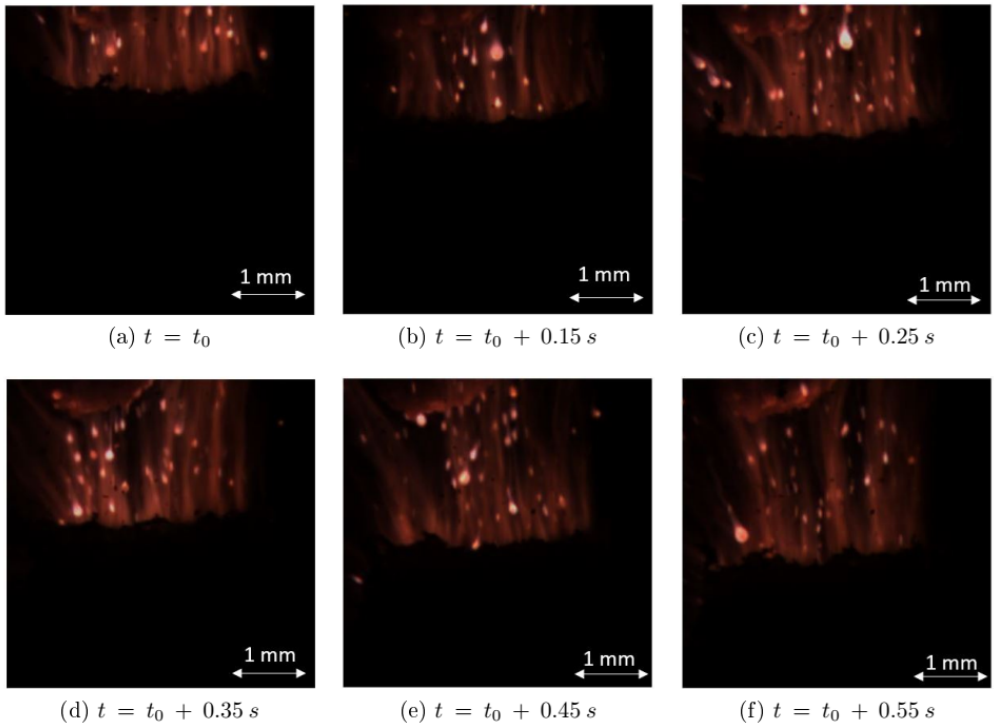

(a) $t = t_0$ (b) $t = t_0 + 0.15\,s$ (c) $t = t_0 + 0.25\,s$

(d) $t = t_0 + 0.35\,s$ (e) $t = t_0 + 0.45\,s$ (f) $t = t_0 + 0.55\,s$

Figure 9: Burning surface visualization sequence for $SP-1$ ($p = 10\ bar$).

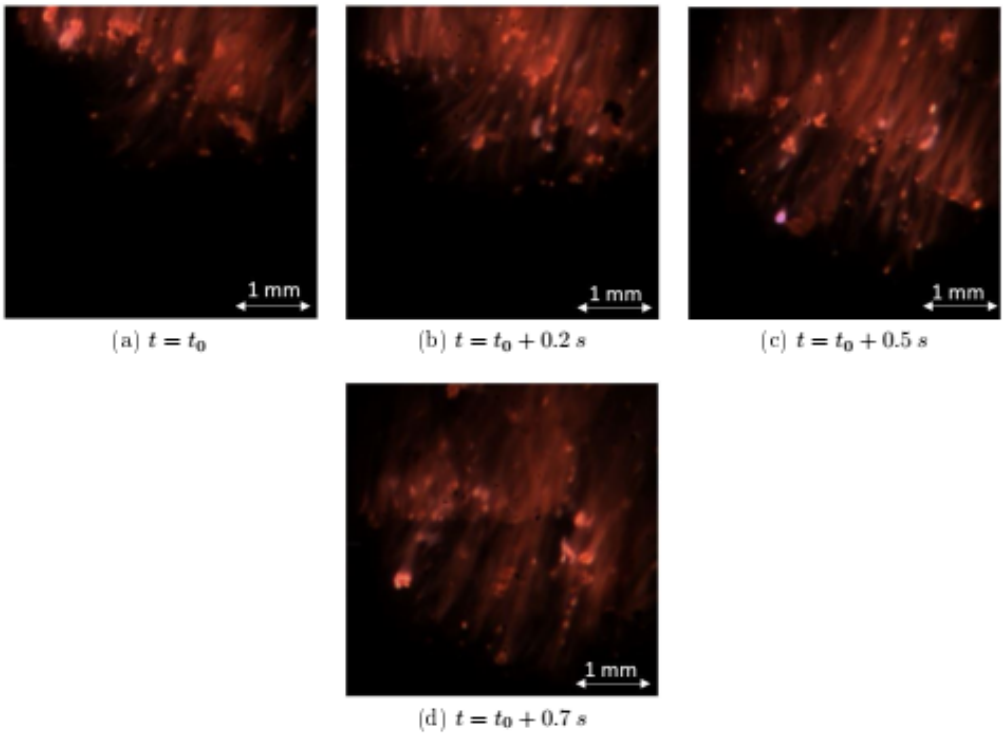

(a) $t = t_0$ (b) $t = t_0 + 0.2\,s$ (c) $t = t_0 + 0.5\,s$

(d) $t = t_0 + 0.7\,s$

Figure 10: Burning surface visualization sequence for $SP-4$ ($p = 10\ bar$).

6. Conclusions and Future Developments

The work presents the results of a joined project between *ReActive - Powder Technology s.r.l.*, *Tomsk State University*, and the *SPLab* of *Politecnico di Milano*. In the study, *Al + Mg* composite fuels produced by *TSU* and *ReActive* are

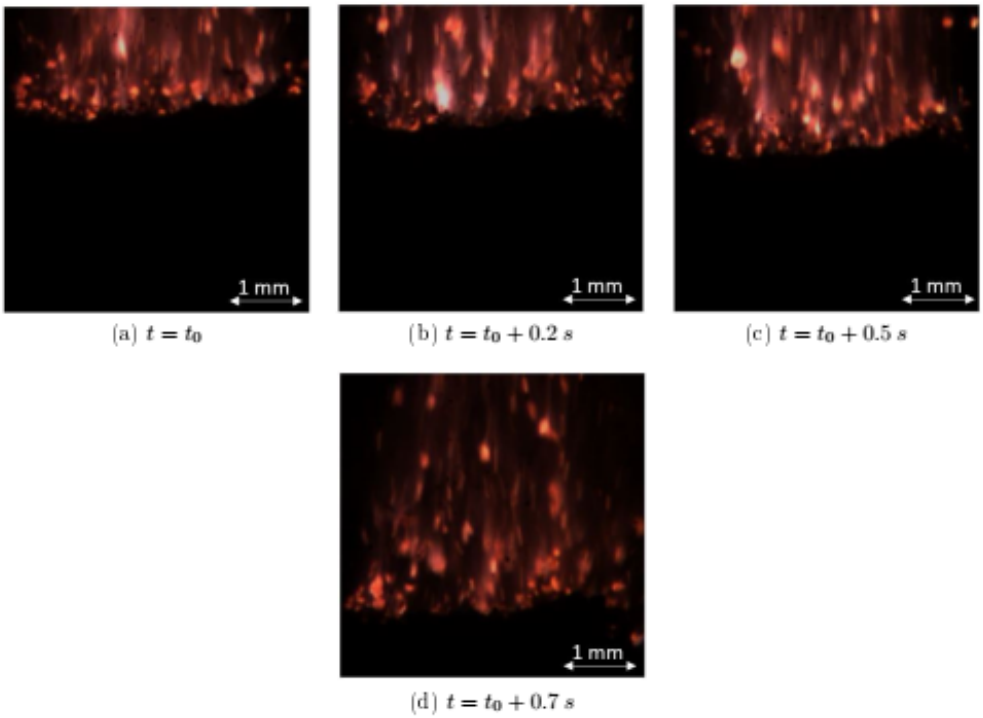

(a) $t = t_0$ (b) $t = t_0 + 0.2\ s$ (c) $t = t_0 + 0.5\ s$

(d) $t = t_0 + 0.7\ s$

Figure 11: Burning surface visualization sequence for $SP - 4B$ ($p = 10\ bar$).

characterized and tested in AP-based propellants. The tested propellants include formulations where the oxidizer is a $AP - PSAN$ blend. The objective of the study is the evaluation of the propellants ballistic response in terms of r_b and $CCP\ D_{43}$. The use of Mg promise a reduction of the HCl produced by AP-based solid propellants. The use of the Cl-free $PSAN$ offer a further possibility for solid propellant environmental impact reduction. The work starts with a theoretical investigation of the impact of Mg and $PSAN$ on the specific impulse performance of commercial solid propellants. While significant HCl reduction is obtained for composite fuels with Mg mass fraction of 50%, when taking specific impulse as a driver for performance, a limitation for the content of the alkaline earth metal to nearly 30 $wt\%$ can be considered. In spite of the relatively low oxygen balance of $PSAN$, a partial substitution with 17 $wt\%$ NH_4NO_3 of the original 68$wt\%$ AP reduces the HCl mass fraction at nozzle throat (from $NASA - CEA$) by 21% (from 18.9 $g/(100\ g)$ to 14.9 $g/(100\ g)$). With the oxidizer blend, the use of a composite fuel with 70 $wt\%$ Al and 30 $wt\%$ Mg promises a 14.4$wt\%$ of HCl at throat. This is further reduced to 9.5 $wt\%$ when the Mg mass fraction in the metal powder rises to 50%. In this latter case, the specific impulse reduces to 3003 m/s, with a -3.0% with respect to the performance of a current commercial propellant. Specific impulse loss is less than 1.0% for the substitution of Al with a composite with 30 $wt\%$ Mg for 68% AP, and 2.1% when considering $AP - PSAN$ blendeed oxidizer with 17 $wt\%$ of $Cl-$free oxidizer. Burning behavior is negatively affected by the $PSAN$ addition to the propellant. For a commercial propellant based on AP (68 $wt\%$) reduction of NH_4ClO_4 to 51 $wt\%$ with 17 $wt\%$ $PSAN$ yields a burning rate reduction of 22.5% when the fuel is Al. The $AlMg$ composites contrast this reduction, providing burning rates comparable with those of the commercial formulation taken as baseline. Further investigation on the impact of the fuel composition on condensed combustion products is needed. Available results suggest, for the composite, flake-like CCP. Yet, this result requires a confirmation exploiting different methods for the analysis of condensed combustion products.

Recommended developments for this work should focus on the evaluation of the impact of the initial powder particle size on the ballistic response of the propellant, and on the determination of the size of condensed combustion products from composite powder combustion. Criticalities in the propellant curing encountered in this work should be considered too, with the definition of strategies to mitigate the impact of this undesirable feature (e.g., powder coating).

References

[1] K. Klager. Polyurethanes, the most versatile binder for solid composite propellants. AIAA Paper No. 1984-1239, 1984.

[2] V. Sekkar and T.S.K. Raunija. Hydroxyl-terminated polybutadiene-based polyurethane networks as solid propellant binder-state of the art. *Journal of Propulsion and Power*, 31(1):16–35, 2015.

[3] N. Kubota. *Propellants and explosives: thermochemical aspects of combustion*. John Wiley & Sons, 2015.

[4] L.T. De Luca, F. Maggi, S. Dossi, M. Fassina, C. Paravan, and A. Sossi. Prospects of aluminum modifications as energetic fuels in chemical rocket propulsion. In *Chemical Rocket Propulsion*, pages 191–233. Springer, 2017.

[5] J.K. Sambamurthi, E.W. Price, and R.K. Sigman. Aluminum agglomeration in solid-propellant combustion. *AIAA Journal*, 22(8):1132–1138, 1984.

[6] V. A. Babuk, V. P. Belov, V. V. Khodosov, and G. G. Shelukhin. Investigation of the agglomeration of aluminum particles during the combustion of metallized composite condensed systems. *Combustion, Explosion and Shock Waves*, 21(3):287–292, May 1985.

[7] L. T. DeLuca, L. Galfetti, G. Colombo, F. Maggi, A. Bandera, V. A. Babuk, and V. P. Sinditskii. Microstructure effects in aluminized solid rocket propellants. *Journal of Propulsion and Power*, 26(4):724–732, July 2010.

[8] L.T. De Luca et al. Aggregation versus agglomeration in metallized solid rocket propellants. *International Journal of Energetic Materials and Chemical Propulsion*, 9(1):91–105, 2010.

[9] V. A. Babuk and N. L. Budnyi. Smoke oxide particles formation at the burning surface of condensed systems. *Acta Astronautica*, 158:264–271, 2019.

[10] V. A. Babuk, N. L. Budnyi, and A. A. Nizyaev. Mathematical modeling of agglomerates evolution. In *Progress in Propulsion Physics – Volume 11*, volume 11, pages 131–148. EDP Sciences, 2019.

[11] V. A. Babuk, V. A. Vasilyev, and M. S. Malakhov. Condensed combustion products at the burning surface of aluminized solid propellant. *Journal of Propulsion and Power*, 15(6):783–793, 1999.

[12] J. Jisna and M. Suresh. Ammonium nitrate as an eco–friendly oxidizer for composite solid propellants: Promises and challenges. *Critical Reviews in Solid State and Materials Sciences*, 42(6):470–498, 2017.

[13] F. Maggi and P. Garg. Fragmentation of ammonium nitrate particles under thermal cycling. *Propellants, Explosives, Pyrotechnics*, 43(3):315–319, 2018.

[14] A. Sossi, E. Duranti, C. Paravan, L. T. DeLuca, A. B. Vorozhtsov, A. A. Gromov, Yu. I. Pautova, M. I. Lerner, and N. G. Rodkevich. Non-isothermal oxidation of aluminum nanopowder coated by hydrocarbons and fluorohydrocarbons. *Applied Surface Science*, 271:337–343, April 2013.

[15] A. Sossi, E. Duranti, M. Manzoni, C. Paravan, L. T. DeLuca, A. B. Vorozhtsov, M. I. Lerner, N. G. Rodkevich, A. A. Gromov, and N. Savin. Combustion of HTPB-Based Solid Fuels Loaded with Coated Nanoaluminum. *Combustion Science and Technology*, 185(1):17–36, January 2013. Publisher: Taylor & Francis _eprint: https://doi.org/10.1080/00102202.2012.707261.

[16] C. Paravan, F. Maggi, S. Dossi, G. Marra, G. Colombo, and L. Galfetti. Chapter Thirteen - Pre-burning characterization of nanosized aluminum in condensed energetic systems. In V.E. Zarko and A.A. Gromov, editors, *Energetic Nanomaterials*, pages 341–368. Elsevier, Amsterdam, January 2016.

[17] W.Q. Pang, Y. Li, L.T. DeLuca, D. Liang, Z. Qin, X. Liu, H. Xu, and X. Fan. Effect of metal nanopowders on the performance of solid rocket propellants: A review. *Nanomaterials*, 11(10), 2021.

[18] S. Cerri, M.A. Bohn, K. Menke, and L. Galfetti. Aging of HTPB/Al/AP rocket propellant formulations investigated by dma measurements. *Propellants, Explosives, Pyrotechnics*, 38(2):190–198, 2013.

[19] C. Paravan, A. Verga, F. Maggi, and L. Galfetti. Accelerated ageing of micron- and nano-sized aluminum powders: Metal content, composition and non-isothermal oxidation reactivity. *Acta Astronautica*, 158:397–406, 2019.

[20] C. Paravan, A. Verga, S. Dossi, F. Maggi, and L. Galfetti. Aluminum powders : aging effects on metal content and thermogravimetry reactivity.

[21] A.B. Vorozhtsov, M.I. Lerner, N.G. Rodkevich, S. Sokolov, E.Y. Perchatkina, and C. Paravan. Preparation and characterization of Al/HTPB composite for high energetic materials. *Nanomaterials*, 10(11):2222, November 2020. Number: 11 Publisher: Multidisciplinary Digital Publishing Institute.

[22] A. L. Breiter, L. Ya. Kashporov, V. M. Mal'tsev, P. F. Pokhil, E. I. Popov, V. I. Pepekin, and A. G. Stasenko. Combustion of individual aluminum-magnesium alloy particles in the flame of an oxidizer-fuel mixture. *Combustion, Explosion, and Shock Waves*, 7(2):186–190, April 1971.

[23] A.L. Corcoran, S. Wang, Y. Aly, and E.L. Dreizin. Combustion of Mechanically Alloyed AlMg Powders in Products of a Hydrocarbon Flame. *Combustion Science and Technology*, 187(5):807–825, May 2015.

[24] H. Belal, C.W. Han, I. E. Gunduz, V. Ortalan, and S.F. Son. Ignition and combustion behavior of mechanically activated Al–Mg particles in composite solid propellants. *Combustion and Flame*, 194:410–418, August 2018.

[25] H. Nie, S. Pisharath, and H. H. Hng. Combustion of fluoropolymer coated Al and Al–Mg alloy powders. *Combustion and Flame*, 220:394–406, October 2020.

[26] W. Ao, Z. Fan, L. Liu, Y. An, J. Ren, M. Zhao, P. Liu, and L.K.B. Li. Agglomeration and combustion characteristics of solid composite propellants containing aluminum-based alloys. *Combustion and Flame*, 220:288–297, October 2020.

[27] F. Maggi, S. Dossi, C. Paravan, S. Carlotti, and L. Galfetti. Role of pressure and aluminum size in solid propellant CCP generation. AIAA Paper No. 2017-5076, 2017.

[28] A. Ilyin, A. Gromov, V. An, F. Faubert, C. de Izarra, A. Espagnacq, and L. Brunet. Characterization of aluminum powders i. parameters of reactivity of aluminum powders. *Propellants, Explosives, Pyrotechnics*, 27(6):361–364, 2002.